Prestroke Proteomic Changes in Cerebral Microvessels in Stroke-Prone, Transgenic(hCETP)-Hyperlipidemic, Dahl Salt-Sensitive Hypertensive Rats

Agnes Bergerat,[1] Julius Decano,[2,3] Chang-Jiun Wu,[4] Hyungwon Choi,[5] Alexey I Nesvizhskii,[5] Ann Marie Moran,[2,3] Nelson Ruiz-Opazo,[2,3] Martin Steffen,[1,6] and Victoria LM Herrera[2,3*]*

[1]Department of Pathology and Laboratory Medicine; [2]Whitaker Cardiovascular Institute; and [3]Department of Medicine, Boston University School of Medicine, Boston, Massachusetts, United States of America; [4]Department of Medical Oncology, Dana-Farber Cancer Institute, Boston, Massachusetts, United States of America; [5]Department of Pathology, University of Michigan, Ann Arbor, Michigan, United States of America and [6]Department of Biomedical Engineering, Boston University, Boston, Massachusetts, United States of America

Stroke is the third leading cause of death in the United States with high rates of morbidity among survivors. The search to fill the unequivocal need for new therapeutic approaches would benefit from unbiased proteomic analyses of animal models of spontaneous stroke in the prestroke stage. Since brain microvessels play key roles in neurovascular coupling, we investigated prestroke microvascular proteome changes. Proteomic analysis of cerebral cortical microvessels (cMVs) was done by tandem mass spectrometry comparing two prestroke time points. Metaprotein-pathway analyses of proteomic spectral count data were done to identify risk factor–induced changes, followed by QSPEC-analyses of individual protein changes associated with increased stroke susceptibility. We report 26 cMV proteome profiles from male and female stroke-prone and non–stroke-prone rats at 2 months and 4.5 months of age prior to overt stroke events. We identified 1,934 proteins by two or more peptides. Metaprotein pathway analysis detected age-associated changes in energy metabolism and cell-to-microenvironment interactions, as well as sex-specific changes in energy metabolism and endothelial leukocyte transmigration pathways. Stroke susceptibility was associated independently with multiple protein changes associated with ischemia, angiogenesis or involved in blood brain barrier (BBB) integrity. Immunohistochemical analysis confirmed aquaporin-4 and laminin-α1 induction in cMVs, representative of proteomic changes with >65 Bayes factor (BF), associated with stroke susceptibility. Altogether, proteomic analysis demonstrates significant molecular changes in ischemic cerebral microvasculature in the prestroke stage, which could contribute to the observed model phenotype of microhemorrhages and postischemic hemorrhagic transformation. These pathways comprise putative targets for translational research of much needed novel diagnostic and therapeutic approaches for stroke.

Online address: http://www.molmed.org
doi: 10.2119/molmed.2010.00228

INTRODUCTION

Stroke is the third leading cause of death and the leading cause of disability in the United States with persistent risk despite successful antihypertensive therapies (1), and minimal efficacy of therapies targeting neuronal loss reduction (2). These unexpected shortfalls highlight the need for the study of the brain microvasculature—composed of the microvascular endothelial cell, basal lamina matrix (BLM), pericyte and astrocyte end feet—in stroke pathogenesis (3,4). Clinical evidence implicating cerebral cortical microvessel (cMV) involvement in stroke pathogenesis are deduced from cumulative MRI-based observations that cerebral microhemorrhages coexist with acute spontaneous intraparenchymal hemorrhages (5,6) and predict new disabling or fatal strokes in patients with acute ischemic stroke or transient ischemic attack (7). Altogether, these associations reiterate the need to study cMVs as they comprise the site for said microhemorrhages.

Given that microvessels are at the frontline of oxidative stress, hypoxia/ischemia and inflammation, and given their key role in the maintenance of the

*VLMH and MS contributed equally as senior authors.

Address correspondence and reprint requests to *Victoria LM Herrera, Whitaker Cardiovascular Institute, Boston University School of Medicine, 700 Albany Street, Boston, MA 02118. Phone: 617-638-4020; Fax: 617-638-4066; E-mail: vherrera@bu.edu; or Martin Steffen, Department of Pathology and Laboratory Medicine, Boston University School of Medicine, 670 Albany Street, Boston, MA 02118. Phone: 617-414-7935; Fax: 617-414-1646; E-mail: steffen@bu.edu.*

Submitted November 16, 2010; Accepted for publication April 13, 2011; Epub (www.molmed.org) ahead of print April 14, 2011.

blood brain barrier (BBB), investigation of cerebral microvascular molecular and cellular changes could contribute critical new insight into mechanisms of stroke pathogenesis. Analysis of cMVs could address the translational roadblock in current stroke intervention strategies, which have focused on large artery pathology and neuronal death. However, owing to their inaccessibility for systematic study in humans and the limitations of *in vitro* systems, analysis of the putative role(s) of cMVs in stroke pathogenesis requires an animal model that recapitulates stroke paradigms which implicate microvascular pathology.

The rat stroke model of ischemic-hemorrhagic stroke induced by early life sodium exposure in an inbred polygenic-hypertensive, transgenic-hyperlipidemic Dahl salt-sensitive (Dahl-S) rat, Tg25sp model with sex-specific differences (8) provides a strategic model for molecular analysis of the cerebral microvasculature. This model is characterized by the presence of both hypertension and hyperlipidemia as risk factors, and by a disease-course continuum that recapitulates multiple paradigms of human stroke, such as nonocclusive carotid artery disease with chronic low-flow ischemia, microhemorrhages and hemorrhagic infarctions (8). This disease course implicates cMVs in the pathogenesis, albeit not as the sole culprit. Because the stroke-prone model used is a genetically identical inbred transgenic rat strain exhibiting a relatively confined temporal disease course (8), the prestroke stage can be defined and studied, thereby validating the study of prestroke events.

Because the BLM contributes to cMV integrity (9), neurovascular unit function (4,10), and because BLM loss has been implicated in cerebral postischemic hemorrhagic transformation (9,11), proteomic analysis is necessary to assess protein changes directly in both BLM and cMV cell components. The shotgun proteomic approach by tandem mass spectrometry provides a strategy to interrogate the microvasculature along the disease course of stroke. Only a few proteomic studies of brain microvessels to elucidate disease mechanisms have been done (12–14).

Studying cerebral microvascular changes in stroke pathogenesis is important since the microvasculature is involved in effective paracrine cross-talk in the neurovascular unit (15), and since they comprise accessible targets for new diagnostic and therapeutic strategies. Using a high-throughput proteomic strategy, we tested the hypothesis that putative changes in cMVs precede the onset of stroke in the stroke-prone Tg25sp model which exhibits carotid artery disease, cerebral microhemorrhages and hemorrhagic infarctions (8). Here, we report cMV prestroke proteomic changes associated with age and stroke susceptibility, respectively, in both male and female stroke-prone rats.

MATERIALS AND METHODS

Stroke-Prone Rat Model of Microhemorrhages and Hemorrhagic Infarction

All animal model studies were done in accordance with the Institutional Animal Care and Use Committee of Boston University School of Medicine, Boston MA, USA. Endpoint euthanasia was accomplished via vital tissue collection under general anesthesia. We used an inbred, Dahl-S rat model of adult-onset ischemic-hemorrhagic stroke with a combination of stroke risk factors: hypertension, hyperlipidemia and early-life sodium exposure (0.4% NaCl) (8). Stroke is induced in both nontransgenic (Tg–) and transgenic (Tg+) Dahl-S rats expressing the human cholesteryl ester transfer protein (CETP), Tg[hCETP]$_{25}$ Dahl-S rats or Tg25 (8,16) maintained in our facility. Littermate male (M) and female (F), Tg+ and Tg– Dahl-S rats were used. Given identical genetic background and developmental programming, the relative stroke susceptibility measured as differences in stroke-onset timepoints is: [Tg+F] > [Tg–F] = [Tg+M], in contrast to minimal to no strokes in [Tg–M] rats (8). We assessed two time points prior to overt evidence of stroke, at 2 months of age and at 4.5 months of age. With the exception of the 4.5-month-old Tg25+F (n = 4 rats), all other study groups had n = 3 rats.

Isolation of Cerebral Cortex Microvessels

Brain microvessels from rat cerebrum were isolated as described (8,17). Isolated cMVs retained on the 40-micron cell strainer were washed off, visualized and photographed to confirm cMV isolation, then quantified by weight. Total protein was isolated from each rat cMV sample and analyzed individually by tandem mass spectral analysis. Diagrams of experimental design are shown in Supplementary Figures 1 and 2.

Separation of Proteins and Mass Spectrometry Analysis

Processing of proteins and tandem mass spectral analysis was done as described (18). Tandem MS/MS spectra were collected for the top 10 ions of each MS scan. Spectra were queried against the rat NCBI RefSeq protein database, downloaded in October 2006. Tandem mass spectra were analyzed using SEQUEST (Thermo Fisher Scientific, Waltham, MA, USA). Proteins were considered present only if two high-scoring unique-sequence peptide matches were achieved in a single gel slice, or if a single peptide was observed at two different charge states in that gel slice. On the basis of previous work evaluating false positive matches for peptide identification (19), we adjusted XCorr scores until the false positive rate of protein identification was empirically determined to be 2%, as calculated by the inclusion of two reversed peptide sequences in a single gel slice. SEQUEST DelCn score was required to be ≥0.08. Raw data are available for anonymous download at proteome.commons.org with the following identifier: hvsCus+PP6NDxmBk+kWQBP3Vjl/8bnGCjUW3g9SYTkWMYFOFFPaK8puJsPx7TgOpA10t9VbBgT9WgaWvPQGGsMUWVvIAAAAAAANafQ== (http://proteomecommons.org).

Pathway-Specific Analysis of Age- and Sex-Specific Changes in cMV Proteome

We employed a metaprotein analytic approach recently developed for relatively sparse mass spectrophotometric proteomic data of phosphorylated protein signatures in lung cancer (20). Analysis of pathway-specific abundance changes utilized the 200 pathways of the Kyoto Encyclopedia of Genes and Genomes (KEGG) database included in the "C2:curated pathways, CP:canonical pathway-set" available in the Molecular Signatures Database (MSigDB, http://www.broadinstitute.org/gsea/msigdb/collections.jsp#C2). As described in Wu *et al*. (20), a metaprotein was defined as a specific linear combination of proteins within a curated pathway protein set. In the first step, for each protein set P, we utilized principal component analysis on the spectral count profiles of all proteins belonging to P in all cMV samples to define eigenvectors that reflect the variation in observed spectral count patterns (21). Principal components were considered only if they explained a significant amount of the variation in metaprotein expression (>30%) and had 20 or more proteins observed in the data. The metaprotein expression is the sum of the counts of individual proteins weighted by the coefficients in the eigenvectors corresponding to the principal components.

Metaproteins with differential expression between two comparative groups for age (4.5-month-olds versus 2-month-olds) and sex (F versus M) were determined based on false discovery rates (FDR) q values less than 0.05. The Pearson correlation coefficient between each protein and the metaprotein was computed to identify those proteins within the protein set that are most responsible for the observed pathway-specific variation. This approach appears to be a novel methodology for performing a variation of "gene set enrichment analysis" (22) on proteomic data, and should be broadly applicable to other types of sparse data. For differentially expressed pathways, we also identified individual members of the pathway that are differentially expressed between queried study groups based on a Kruskal-Wallis (KW) rank sum test P value <0.05.

Hierarchical Model-Based Analysis of Proteomic Changes Associated with Stroke Susceptibility

Protein expression was compared between stroke-susceptible and non–stroke-susceptible rats at 4.5 months of age to distinguish differential expression unique to progressive stages of stroke susceptibility in the spTg25 rat model (8). The stroke-susceptible group spanned three sets of rats that exhibited stroke: Tg+ males, Tg+ females, Tg– females (n = 3 per set for each time point). The non–stroke-prone group is composed of littermate Tg– males (n = 3 set for each time point).

The QSPEC method by Choi *et al*. (23) was used for the statistical inference for differential protein expression from spectral counts, with a modification that accounts for proteomic changes due to sex- and transgenic CETP-induced hyperlipidemia. QSPEC is a hierarchical model-based method for statistical inference of spectral count-based differential protein expression (23), parallel to gene set enrichment analysis of transcription profiles (22). Two statistical models are fit in each protein: $(M_{1i})\ Y_{ij} = \beta_{0i} + \beta_{1i}C_j + \beta_{2i}\,G_j + \beta_{3i}T_j$ and $(M_{0i})\ Y_{ij} = \beta_{0i} + \beta_{1i}C_j + \beta_{2i}G_j$, where Y_{ij} denotes the spectral count of protein i in rat j, C_j is the CETP mutation of rat j (1 if transgenic, 0 otherwise), G_j is the gender of rat j (1 if female, 0 if male), and T_j is the stroke susceptibility (1 if susceptible, 0 otherwise). The differential expression status is indicated by the presence or the absence of parameter β_{3i}. Given the two candidate models, differential expression for protein is tested based on the magnitude of Bayes factor (BF), defined by a likelihood ratio of the two models, that is, $BF_i = P(M_{1i} \mid Y_i) \mid P(M_{0i} \mid Y_i)$ (24). Large BF supports the hypothesis of differential expression for the protein.

By following conventional suggested guidelines (25), proteins with BF ≥30 were selected as differentially expressed. Induced and de-induced proteins associated with stroke susceptibility were separately listed. In addition, proteins with evidence of confounding by sex and CETP transgene status were removed from the candidate list, which was also examined by their corresponding BF for the two parameters β_{1i} and β_{2i}. Proteins were not included in the list of differentially expressed proteins associated with stroke-susceptibility if they also exhibited a BF ≥30 for sex (F or M) or transgenic hyperlipidemia status (Tg+ or Tg–).

Immunohistochemical Analysis of Rat Brain Sections

Histological processing and immunohistochemical analyses were done as described (8) (Supplementary Information-Methods for specific details).

All supplementary materials are available online at www.molmed.org.

RESULTS

Cerebral Microvascular Proteome—Insight into the Blood Brain Barrier

To determine proteins and pathologic processes associated with increased stroke susceptibility, we used 1D-PAGE/LC/MS/MS spectrometry (18) to obtain total proteome profiles from cerebral cortex microvessels (cMVs). We reduced the complexity of stroke proteomes by focusing on changes in isolated cerebral microvascular proteomes rather than the whole brain. We studied rat subgroups which represent the spectrum of stroke susceptibility including the nonstroke phenotype. Stepwise analyses of cMV proteomes were done to distinguish proteomic changes due to specific risk factors and those associated with stroke susceptibility independent of said risk factors. We obtained cMV samples from inbred stroke-prone Tg[hCETP]25 Dahl S rat model, thus eliminating confounders from genetic heterogeneity and environmental factor variation. We obtained and studied cMV proteomes from eight rat

groups with varying combinations of the major risk factors observed in this model: age, sex and combined hypertension-hyperlipidemia, all of which contribute to stroke susceptibility as measured by earlier stroke onset (8). The effects of these risk factors on the cMV proteome were analyzed separately to gain insight into risk factor–induced pathogenic mechanisms. Thereafter, exclusion of these proteins differentially expressed with respect to age, sex or transgenic status allowed the identification of those proteins which change specifically with stroke susceptibility. (Experimental design scheme shown in Supplementary Figures 1 and 2.)

In total, we report 26 proteome profiles (Table 1). The average number of proteins identified from each rat within each group is summarized (Table 1) with the comprehensive listing of proteins per sample in Supplementary Table 1. We identified 1,934 proteins by two or more peptides in the 26 samples. Many proteins were observed in most or many of the samples: 637 proteins were identified in 20 or more samples, 1,033 were identified in 10 or more. Only 122 proteins of the 1,934 total were identified only in a single sample.

We also report the detection of relatively similar spectral counts among all cMV samples of some proteins characteristic of endothelial cells (ACE2, vWF), BLM (collagen [COL]-18A1, COL-6A2, COL-6A3, nidogen-1 and -2), pericytes (smooth muscle α actin) and astrocyte end feet (GFAP) (data not shown), thus indicating that cMVs isolated using the brain microvessel procedure (17) represent the BBB. The BBB is composed of the microvascular endothelial cell, BLM, pericytes and astrocyte end feet (26). This characterization of cMV composition is concordant with the analysis of "brain microvessels" isolated by laser capture microdissection which detected identical multicellular composition (12,27). Unsupervised cluster analysis confirms the multiple cell types and ECM representation of the BBB in all cMV samples (data not shown). Importantly, the detection of these proteins with similar spectral counts in all cMV samples indicate relatively similar BBB cell composition of cMV samples, thus validating the proteomic analysis of cMVs and the detection of differentially expressed proteins. We also note that some cMV isolates had red blood cell (rbc) contamination, and these rbc-specific proteins, such as hemoglobin and carbonic anhydrase-1 were excluded (data not shown).

Table 1. Number of proteins detected per study group by proteomic analysis.

Group number	Number of rats studied	Sex	Age (months)	CETP transgene[a]	Lipid levels[b]	BP[c]	Stroke susceptibility[d]	Number of proteins observed	CV[e] (%)
1	3	M	2	–	nl	Pre	–	979	2.5
2	3	M	2	+	+	Pre	–	1,063	2.9
3	3	F	2	–	nl	Pre	–	1,021	9.6
4	3	F	2	+	±	Pre	–	1,024	2.6
5	3	M	4.5	–	nl	Hyp	–	1,082	5.1
6	3	M	4.5	+	+++	Hyp	+	1,052	8.3
7	4	F	4.5	–	nl	Hyp	++	1,177	6.7
8	4	F	4.5	+	+	Hyp	+++	1,063	14.6
Total	26							1,058 (avg[f])	5.5 (avg)

[a]+, Human CETP transgene–positive expression; –, nontransgenic.
[b]+, Mild increase in total plasma cholesterol (TC) and total plasma triglyceride (TG) as observed previously (8); ++, moderate increases in TC and TG as observed previously (8); +++, moderate-severe increases in TC and TG as observed previously (8); nl, normal; ±, minimal increase in TC and TG levels
[c]BP, blood pressure; Pre, prehypertensive; Hyp, moderate-severe hypertension.
[d]+, ++, +++: Increasing stroke susceptibility marked by earlier onset.
[e]CV, coefficient of variation.
[f]avg, Average.

Differential Effects of Age and Hyperlipidemia on the cMV Proteome

We next analyzed cMV proteomic changes associated with age or hyperlipidemia. Integrating a functional context to our proteomic analysis, we used a pathway-based analytic approach developed for proteomic spectral counts with the pathway protein set serving as the metaprotein and validated previously for relatively sparse phosphoproteomic data (20). We explored pathway differences between 2-month-old and 4.5-month-old rats. Because most stroke-prone Tg+ female rats succumb to stroke at 4 to 5 months, we were unable to study a later time point. At 2 months, blood pressure and total plasma cholesterol and total plasma triglyceride levels are equivalent and normal between male and female rats, and stroke events are not detected (8). In contrast, at 4.5 months, hypertension is moderate to severe in both Tg+ and Tg– rats exposed to early life sodium (0.4% NaCl), while hyperlipidemia is present in Tg+ rats but not in Tg– rats, with Tg+ female rats exhibiting far less hyperlipidemia than males (8,16; Supplementary Figure 3). Because all 4.5-month-old rats are compared with 2-month-old rats regardless of sex, transgenic-hyperlipidemic phenotype and stroke predisposition in this 2-month versus 4.5-month analysis subset, differentially expressed proteins reflect age-associated changes rather than stroke susceptibility.

Metaprotein analysis using 200 KEGG pathways listed in the canonical pathway database (MSigDB) identified differential expression between 2-month-old and 4.5-month-old rats in six metaproteins or KEGG pathways within two unifying cat-

Table 2. Differentially expressed pathways with age: cMVs of 4.5-month-old versus 2-month-old rats.

Pathways[a]	FDR[b]	Protein ID[c]	Pearson correlation *P* value[d]	4.5- versus 2-month-old rats[e]	KW *P* value[f]
Energy metabolism					
HSA00010 glycolysis and gluconeogenesis	0.010	ALDH2: aldehyde dehydrogenase 2	0.019	↓	0.004
		LDHB: lactate dehydrogenase 2	0.007	↓	0.005
		ALDOC: aldolase C	9.1×10^{-4}	↑	0.050
		ENO2: enolase 2	1.4×10^{-5}	↑	0.037
		HK1: hexokinase 1	4.2×10^{-7}	↑	4.7×10^{-5}
		PFKP: phosphofructokinase, platelet	0.045	↑	1.9×10^{-3}
		PKM2: pyruvate kinase, muscle	7×10^{-7}	↑	0.017
HSA00020 citrate cycle	0.011	MDH2: malate dehydrogenase 2	6×10^{-32}	↓	1.7×10^{-3}
		ACLY: ATP citrate lyase	4×10^{-4}	↑	1.7×10^{-3}
		DLST: dihydrolipoamide S-succinyltransferase	1×10^{-3}	↑	0.017
HSA00620 pyruvate metabolism	0.011	ALDH2: aldehyde dehydrogenase 2	0.034	↓	0.004
		LDHB: lactate dehydrogenase B	0.011	↓	0.005
		MDH2: malate dehydrogenase 2	0.000	↓	1.7×10^{-3}
		PDHB: pyruvate dehydrogenase β	3×10^{-5}	↓	0.057
Cell-microenvironment interactions					
HSA01430 cell communication	0.011	ACTG1: actin, γ 1	0.002	↓	0.007
HSA04512 ECM-receptor interaction	0.056	VIM: vimentin	2.8×10^{-9}	↓	0.002
		COL1A1: collagen, type I, α1	5.8×10^{-5}	↑	0.016
		COL4A2: collagen, type IV, α2	1.3×10^{-4}	↑	0.017
		LAMA1: laminin, α1	1.5×10^{-9}	↑	0.019
		LAMA5: laminin, α5	1.1×10^{-8}	↑	0.027
		LAMB2: laminin, β2	3.8×10^{-11}	↑	0.035
		TNR: tenascin R	1.4×10^{-3}	↑	0.004

[a]Numbered KEGG canonical pathways.
[b]FDR, false discovery rate with significance defined as FDR <0.05.
[c]Entrez Gene official symbol. Proteins may exist in multiple overlapping pathways; e.g., LAMA1 is a component of both cell communication and ECM-receptor interaction pathways.
[d]Pearson correlation $P < 0.05$, identifies proteins within the pathway protein set that are most responsible for the observed pathway-specific variation.
[e]See footnote f for information on the arrows.
[f]Kruskal-Wallis rank sum test of individual proteins in differentially expressed pathway identifying individual proteins that are increased (↑) or decreased (↓) in 4.5-month-old rat cerebral microvessels.

egories: 1) energy metabolism, and 2) cell-microenvironment interactions. All pathways listed exhibited significant differences with false discovery rates (FDR) ≤0.05 (Table 2). Among differentially expressed energy metabolism metaproteins, the glycolysis pathway is increased while the citrate cycle and pyruvate metabolism pathways are decreased (Table 2). Among cell–microenvironment interaction metaproteins, the cell communication pathway is decreased and a net increase in ECM-receptor interaction pathway is observed (Table 2). Furthermore, several proteins within each pathway-specific protein set exhibited significant correlation to metaprotein changes (Pearson correlation $P < 0.05$) and statistically significant differences (KW $P < 0.05$) between 4.5-month-old and 2-month-old rat cMV proteomes.

Surprisingly, transgenic hyperlipidemia did not induce significant pathway changes in cMV proteomes using false discovery rate (FDR) analysis (Supplementary Table S2). We note, however, that the top scoring pathway, ECM-receptor interactions, had individual proteins whose expression levels varied significantly ($P < 0.05$) and also correlated with the metaprotein (Pearson correlation $P < 0.05$) (Supplementary Table S2).

Pathways Differentially Expressed between Males and Females

To gain insight into putative mechanisms that underlie greater stroke susceptibility in female rats compared with males despite equivalent levels of hypertension and less hyperlipidemia, and a lower risk for coronary artery disease (8), we analyzed male-to-female differences for young, old and both age groups combined. We obtained qualitatively similar results for both age groups, but the highest statistical significance was detected in the 4.5-month-old rat groups and are reported here (Table 3).

Table 3. Differentially expressed pathways in 4.5-month-old female versus male rat cMVs.

Pathways[a]	FDR[b]	Protein ID[c]	Pearson correlation *P* value[d]	F versus M[e]	KW *P* value[f]
HSA00010 glycolysis and gluconeogenesis	0.040	PKM2: pyruvate kinase, muscle	0.003	↓	0.007
		ENO2: enolase 2	1.3×10^{-3}	↓	0.014
		AKR1A1: aldoreductase family 1	1.2×10^{-3}	↓	0.019
		ALDOC: aldolase C	1.1×10^{-3}	↓	0.028
HAS04670 leukocyte transendothelial migration	0.040	VCL: vinculin	6.1×10^{-4}	↑	0.014
		ITGB1: integrin, β1	0.006	↑	0.024

[a]Numbered KEGG canonical pathways.
[b]False discovery rate with significance defined as FDR <0.05.
[c]Entrez Gene official symbol.
[d]$P < 0.05$ identifies proteins within the pathway protein set that are most responsible for the observed pathway-specific variation.
[e]4.5-month-old female versus male rat cMVs. See footnote f for information on the arrows.
[f]Kruskal Wallis rank sum test of individual proteins in differentially expressed pathway identifying individual proteins that are increased (↑) or decreased (↓) in 4.5-month-old female cMVs.

Two KEGG pathways/metaproteins exhibited significant differential expression—HSA00010 glycolysis and gluconeogenesis pathway and HSA04670 leukocyte transendothelial migration pathway (Table 3). In 4.5-month-old females, the glycolysis/gluconeogenesis metaprotein exhibited a decrease (FDR = 0.04) in contrast to 4.5-month-old males (Table 4). This decrease is opposite of the increase observed with aging (Table 2). Individual protein analyses detected five proteins with significant correlation with the metaprotein (Pearson $P < 0.002$) and significant differences between sexes (KW $P < 0.05$) (Table 3). Interestingly, 3 of the 5 proteins decreased in the female-specific glycolysis pathway protein set are increased in the protein set for the age-associated change in glycolysis/gluconeogenesis pathway, PKM2, ENO2 and ALDOC (Tables 2,3). The proteins detected to be changed significantly between comparative groups and correlated with differential expression of the leukocyte transendothelial migration pathway are vinculin and integrin β-1 (Table 3).

Differentially Expressed Proteins in Stroke-Prone Cerebral Microvessels

Having analyzed the proteomic changes associated with age, sex-specific differences and hyperlipidemia, we next assessed cMV proteome alterations that are associated with stroke susceptibility independent of said risk factor–induced changes. We limited the analysis to 4.5-month-old rats to maximize differences in stroke susceptibility as observed (8). We utilized QSPEC to identify differentially expressed proteins (23) as indicated by statistically significant differences in spectral counts (28). We identified proteins that varied as a function of stroke susceptibility using analysis of variance (ANOVA), eliminating protein changes associated with sex-specific differences or hyperlipidemia given that the latter two, while risk factors, also are confounding variables. Analysis was limited to 4.5-month-old rats that are closer temporally to stroke onset, and because 2-month-old rats do not display a hyperlipidemic profile yet (8). We report proteins that were significantly different between non–stroke-prone and stroke-prone 4.5-month-old rats (Table 1, group 5 versus groups 6,7,8), but not between nontransgenic-normolipidemic rats and transgenic-hyperlipidemic rats (Table 1, groups 5,7 versus groups 6,8), and not between male and female 4.5-month-old rats (Table 1, groups 5,6 versus groups 7,8) (Supplementary Figure 2). With use of QSPEC analysis (23), proteins that exhibit BFs greater than 65 (>65) for the first comparison, but less than 30 for the transgenic-hyperlipidemia and sex, comparisons were considered as associated with stroke susceptibility. By using these criteria, stroke susceptibility is associated with 12 proteins that are increased (Table 4), and 14 that are downregulated (Supplementary Table S3).

Analysis of putative pathogenic implications of the protein set associated with stroke susceptibility was limited to induced proteins (Table 4) since net de-induction could simply be due to loss from cell death. Interestingly, 6 of 12 proteins in the induced-protein set have been reported previously to be increased in ischemia or hypoxia, and/or associated with proapoptosis effects (Table 4), and known to be present in endothelial cells or astrocytes. Additionally, 9 of 12 proteins have been reported to be part of the BBB and their increase would be expected to alter BBB function, as well as result in loss of BBB integrity promoting either brain edema or leukocyte transmigration as observed in strokes. Five induced genes have proangiogenic functions (Table 4) consistent with the notion of ischemia-induced angiogenesis. Altogether, this protein set indicates ongoing molecular changes in cMVs prior to the onset of stroke which could be expected to contribute to stroke susceptibility and post-stroke sequelae.

Table 4. Proteins induced with increased stroke susceptibility in 4.5-month-old rats.

Protein ID[a]	Bayes Factor: SP versus nonSP[b]	Bayes Factor: Tg+ versus Tg–[c]	Bayes Factor: F versus M[d]	Protein name	cMV site: E[e]	cMV site: M[f]	cMV site: P[g]	cMV site: A[h]	Pathogenic Pathway: Ischemia/hypoxia; cell death/death	Pathogenic Pathway: Angiogenesis	Pathogenic Pathway: BBB structural and functional integrity
AQP4	4,155,184	13	0	Aquaporin 4	E			A	Increased in ischemia (36)		Increased in brain edema (36)
SLC2A1	16,731	1	1	Glucose transporter-1	E			A	Increased in ischemia, hypoxia metagene (37)		
GNAI2	6,941	1	4	G-protein α12	E						Mediates thrombin induced EC permeability (38)
COL12A1	2,780	1	12	Collagen XII		M					BBB integrity; increased in ECs by shear stress (39)
CA4	1,798	11	1	Carbonic anhydrase-4	E			A	Increased in hypoxia/ anoxia (40)		Buffers brain extracellular space (41)
SLC9A3R2	1,391	7	11	NHE-3 regulator-2	E				Enhances PDGF-induced proliferation (42)	Procell migration (43)	PDZ scaffold, anchors ion channels and receptors to cytoskeleton (44)
ANPEP	1,258	1	1	Aminopeptidase-N	E		P			Proangiogenesis (45)	
KRAS	233	2	2	K-ras				A	Increased pK-ras in hypoxia, blocks apoptosis (46)	Proangiogenesis (46)	
SNTA1	191	3	0	Syntrophin, α1				A			Anchors AQP4 in astrocyte end feet (29)
FLNB	113	3	1	Filamin B	E					Proangiogenesis (47)	Mediates ICAM-1 driven wbc transendothelial migration (48)
TF	73	1	24	Transferrin	E				Iron accumulation causes oxidative stress and neurodegeneration (49)		Antioxidant sequestration of iron (50)
LAMA1	69	9	2	Laminin α1	E	M				Proangiogenic peptides from lama1 (51)	Key component of BLM

[a]Entrez Gene official symbol.
[b]Stroke-prone versus non–stroke-prone cMVs.
[c]Transgenic-positive versus transgenic-negative cMVs.
[d]Female versus male cMVs.
[e]cMV endothelial cells.
[f]cMV BLM.
[g]cMV pericytes.
[h]cMV astrocyte end feet.

Confirmation of Aquaporin-4 and Laminin-α1 Protein Changes

To confirm proteomic changes associated with stroke susceptibility, we studied AQP4 and laminin-α1 by immunohistochemical analysis of serial rat brain sections from stroke-prone and non–stroke-prone rats. AQP4 and laminin-α1 were selected because they represent the proteins with the highest and lowest BF with significance cutoff >65 BF for association with stroke susceptibility, in contrast to <30 BF for either age or sex (Table 4).

In contrast to non–stroke-prone rat brains (Figure 1A–D), AQP4 and laminin α1 immunostaining exhibited increased signal intensity and spatial distribution in stroke-prone rat arteriolar and postcapillary venular microvessels (Figure 1E–H). Similarly, in contrast to capillary microvessels in non–stroke-prone rat brains (Figure 2A, C), AQP4 also exhibited increased signal intensity and spatial distribution in cMV capillaries (Figure 2D, F). These immunohistochemical observations confirm the proteomic changes associated with stroke susceptibility (Table 4). Additionally, proteomic spectral count analysis of proteins that anchor AQP4 in the dystrophin complex to the perivascular membrane of astrocyte end feet revealed that key anchoring components are present in the cMV proteome: dystroglycan, α1-syntrophin, dystrophin-isoform Dp71, and dystrobrevin-α (Supplementary Table 1), thus supporting the detection of AQP4 in cMV samples. Moreover, α1-syntrophin also is increased in association with stroke susceptibility (Table 4). Interestingly, AQP4 is increased in arteriolar astrocyte end feet, while increased AQP4 appears to be increased in either or both astrocyte end feet and endothelium in postcapillary venules and capillaries, since light microscopy cannot distinguish the two, and since abluminal apposition of AQP4 immunostaining to endothelial nuclei suggest abluminal endothelial-membrane localization (Figure 1C, G; 2D 2F). Endothelial AQP4 expression has been reported, with greater amounts in

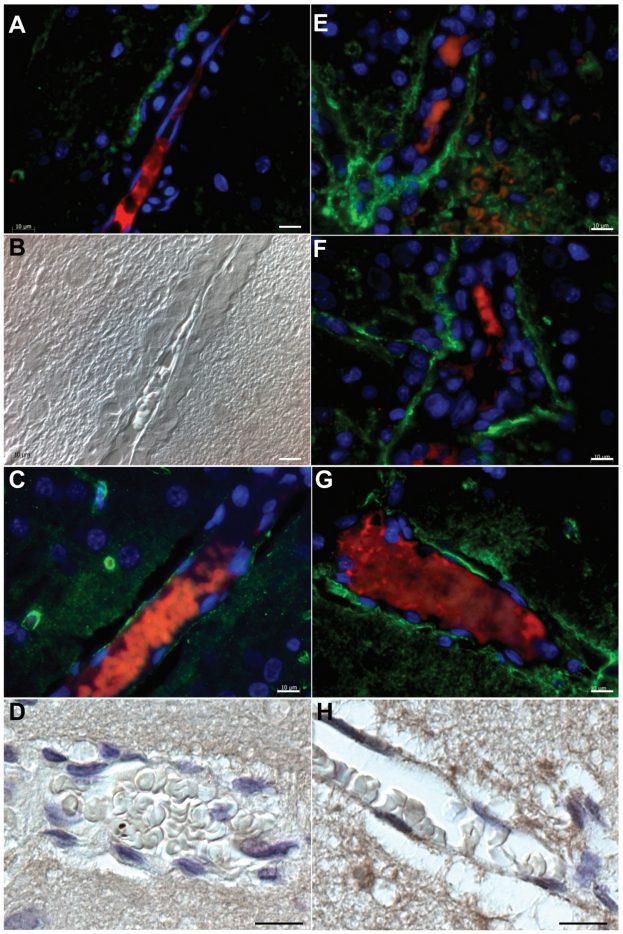

Figure 1. Representative immunohistochemical analysis of AQP4 and laminin-α1 expression in cerebral cortex 20- to 30-micron microvessels (cMVs). (A–D) control, non–stroke-prone rat brains; (E–H) stroke-prone rat brain sections. (A) AQP4-positive immunostaining (green) is detected on one side of an arteriolar cMV BLM in an 18-month-old non–stroke-prone rat. RBCs exhibited red autofluorescence within the cMV lumen in the presence of double immunostaining with AF594-fluorophore (red) labeled glial fibrillary acidid protein (GFAP). DAPI-stained nuclear DNA (blue) highlights the flat-ellipsoid nuclei of endothelial cells (ECs) lining the cMV lumen, with no AQP4 expression. DAPI-stained, round pericyte nuclei are detected between ECs and AQP4-positive staining, consistent with astrocyte–end feet expression of AQP4. (B) Diffusion contrast interference (DIC) image depicts structural outline of 25–30 micron cMV in panel A, confirming cMV lumen with red blood cells. (C) Double immunostaining of AQP4 and AF594-labeled rat endothelial cell antigen1 (Reca1) detects partial AQP4 immunostaining in abluminal side of endothelial cells lining an ~20 micron-cMV lumen in a non–stroke-prone 4.5-month-old female rat. Reca1-immunostaining (red) is not detected in cMV endothelium; red autofluorescence is noted in RBCs. (D) Minimal to no laminin α1 (Lama1) DAB-immunostaining (brown) of non–stroke-prone rat cMV. Hematoxylin-stained (blue), flat-ellipsoid EC-nuclei line cMV lumen filled with RBCs. (E,F) Increased intensity and distribution of AQP4 immunostaining is detected bordering both sides of cMV consistent with astrocyte–end feet localization. Reca1-immunostaining (red) is not detected in cMV endothelium; red autofluorescence noted in RBCs. (G) Increased intensity and distribution of AQP4 immunostaining borders both sides of cMV and abuts EC nuclei on the abluminal side. Reca1-immunostaining (red) is not detected in cMV endothelium; red autofluorescence noted in RBCs. (H) Laminin α1-immunostaining (brown) of ECs and BLM is detected in stroke-prone rat cMV. Hematoxylin-stained (blue), flat-ellipsoid EC-nuclei line cMV lumen with RBCs. Bar: 10 microns in panels A–H.

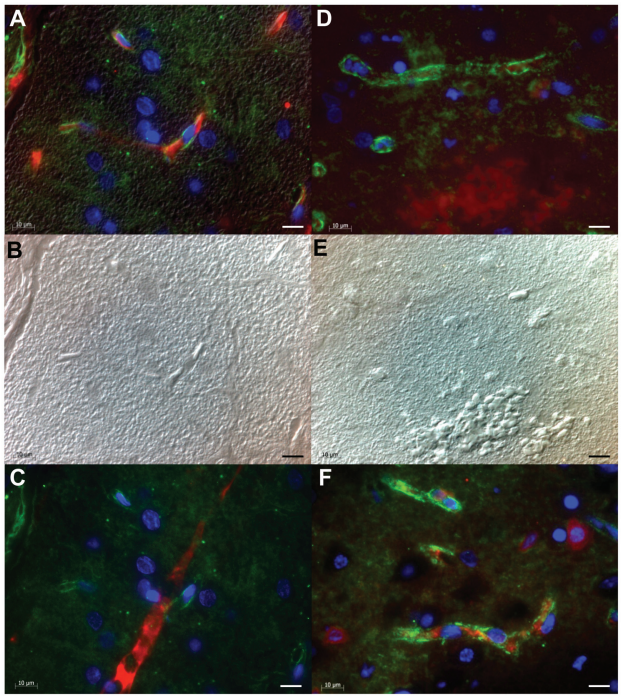

Figure 2. Representative immunohistochemical analysis of AQP4 expression in cortical microvascular capillaries (<10 microns). (A) Double immunofluorescence analysis with AQP4 and GFAP detects low level AQP4-positive immunostaining (green) of cMV capillary endothelium (lining lumen), negative GFAP immunostaining, and RBC red autofluorescence in young 2-month-old stroke-prone rat capillaries. (B) DIC image of panel A showing capillaries. (C) Double immunofluorescence analysis of AQP4 (green) and Reca1 (red) detects minimal to no AQP4 expression in capillaries in non–stroke-prone rat brain and no Reca1 immunostaining. Red autofluorescence of RBCs is noted. (D) Double immunostaining detects increased AQP4-positive immunostaining of cerebral microvessel poststroke in a 4.5-month-old stroke-prone rat brain close to a microhemorrhage with red autofluorescence of extravasated RBCs in the cortical parenchyma. (E) DIC image of panel 2D showing capillaries and microhemorrhage. (F) Increased AQP4 immunostaining in cortical capillaries (≤10 microns) with red autofluorescence of luminal RBCs. DAPI-nuclear DNA stain (blue) Bar: 10 microns for panels A–F.

the abluminal compared with the adluminal endothelial membrane (29).

DISCUSSION

Importance of Direct Study of cMV Proteomes

Focus on rat stroke model-derived cMV proteomes is important since there is no *in vitro* system that can recapitulate the critical cell-to-cell and cell-to-matrix interactions in intact cMVs nor recapitulate molecular-to-cellular events in stroke pathogenesis. Additionally, studying the status of cMV proteomes per se gives insight into its critical roles in the maintenance of BBB integrity and neurovascular coupling (4). Detection of distinct pathways with differential expression is contrasted to the many more pathways not exhibiting statistically significant differential expression, thus giving compelling confidence to detection of said observed changes (Tables 2–4).

Insight into Risk-Factor Induced Prestroke Changes in cMVs

Metaprotein analysis identified increased glycolysis-pathway in 4.5-month-old rats compared with 2-month-old rats, similar to increased glycolysis associated with hypoxia (30). On the other hand, sex-specific proteome analysis also detected increased expression of glycolysis pathway proteins in 4.5-month-old male rats, which have been observed to have less stroke susceptibility than female rats. These seemingly conflicting observations can be reconciled with the hypothesis that while increased glycolysis indicates relative low grade ischemia/hypoxia as rats age, males have the advantage over females because the increase in glycolysis pathway proteins is thought to be an adaptive compensation seen in astrocytes but not in neurons. The ability of astrocytes to compensate and restore mitochondrial membrane potential through glycolytically generated ATP allows them to resist apoptosis in chronic low flow ischemia in contrast to neurons, which are unable to increase glycolysis for energy demands during hypoxia, and hence proceed to apoptosis given ischemia/hypoxia (30). Altogether, the greater increase in glycolysis pathway protein set in 4.5-month-old males could give them a compensatory advantage over 4.5-month-old females, thus accounting for the greater susceptibility in females (8). Additionally, 4.5-month-old females also exhibited a significant increase in the leukocyte transmigration pathway compared with male cMVs, concordant with the observation of greater stroke susceptibility in females as observed in stroke-prone Tg25 rat model (8).

Insight into Putative Stroke-Prone Pathogenic Mechanisms

Prestroke changes in cMV basal lamina matrix. In contrast to the analysis of RNA changes, proteomic analysis of cMVs gives a direct analysis of the cumulative net changes in the BLM of the cMV which is produced and modulated by all three cellular components of the BBB—endothelial cell, pericyte and astrocyte. Elucidation of changes in the BLM provides insight into intercellular cross-talk within the BBB and, even more importantly, within the neurovascular unit, which impacts not just the integrity of microvascular permeability, but also neurovascular coupling, neutro-

transmitter inactivation, neurotrophic coupling and angiogenic and neurogenic coupling (31). More specifically, the detected net increase in collagen-12A1 and laminin-1 associated with stroke susceptibility suggests the hypothesis that altered basement membrane composition and amount could lead to a loss of the ability of the vessels to autoregulate in response to changing hemodynamic conditions, thus leading to chronic low flow ischemia and vulnerability to microhemorrhages and/or postischemic infarction hemorrhagic transformation (8). These stroke susceptibility-specific changes are reinforced with ECM-receptor-interaction pathway changes independently induced by age, thus altogether leading to changes in the collagen network affecting 4 types of collagen, COL12A1, COL4A1, COL4A2 and COL1A1, and the laminin network affecting several laminin isoforms: LAMA1, LAMA5, LAMB2 (Table 2).

Prestroke pathway changes associated with stroke susceptibility. Concordantly, proteins that are increased in association with stroke susceptibility are known to be expressed in the different BBB cell types: ECs, pericytes or astrocytes (Table 4). Induced cMV proteins that are associated previously with ischemia (Table 4) confirms the presence of chronic low flow ischemia first detected in this stroke-prone rat model by magnetic resonance microimaging (8). Elucidation of significant proteomic changes in the prestroke stage confirms the pathogenic role of low flow ischemia in this stroke-prone Tg25 rat model. Additionally, proteomic changes which can lead to changes in BBB integrity be it edema, leukocyte transmigration or BBB dysfunction (Table 4), provide molecular insight into putative mechanisms that could contribute to the observed stroke features of neutrophil transmigration, microhemorrhages and/or predisposition to hemorrhagic transformation as observed in this model (8).

The association of stroke susceptibility with increased AQP4 expression in both spatial distribution and intensity, in all cMV components (arterioles, postcapillary venules and capillaries, as well as in both astrocyte end feet and abluminal endothelium) altogether suggests the following hypotheses: first, that AQP4 increase in astrocyte end feet provides a molecular mechanism for a preset vulnerability to poststroke brain edema that is initiated at the prestroke stage and not just at the onset of stroke, since AQP4 is the major water channel underlying brain water balance and implicated in ischemic cytogenic edema (32). Secondly, although the role of endothelial AQP4 has not been elucidated, we hypothesize that parallel to known AQP4 roles in astrocytes (32–34), AQP4 increases in stroke-prone cMV venular and capillary endothelia also result in altered water-ion homeostasis and signaling in said cMV endothelium. This perturbation could then contribute to endothelial dysfunction with cascading effects on the neurovascular unit, thereby resulting in altered neurovascular coupling. The resultant putative dysfunction of neurovascular coupling then sustains, if not worsens, the chronic low grade ischemia observed in the stroke-prone, hypertensive rat strain, which coupled with AQP4-mediated cytogenic edema, together contribute to stroke-susceptibility. These hypotheses are supported by observations of increased AQP4 in stroke-prone SHRSP rats (35) and in poststroke human brains with cerebral infarction (36), and by the detection of a hypoxia inducible factor-1α response element in the 5′ flanking region of the human *AQP4* gene.

Limitations of the study. While key insights were obtained, delineation of limitations of the study that could impact biological context of observations is important. Shotgun proteomic analysis by tandem mass spectrometry is limited by the smaller total number of proteins analyzed compared with transcription profiling. Hence while positive findings are informative, nondetection of a protein does not equate with noninvolvement in stroke susceptibility. As with all "-omics" analysis of complex tissues valued for critical biological context, detection of protein level alterations not caused by cell composition changes does not pinpoint cell-specific origin(s) of said changes. Additionally, the temporal variation in disease course of adult-onset stroke models, despite identical genetic backgrounds, adds further variability onto the inherent variation in shotgun proteomic analysis by tandem mass spectrometry, thus reiterating that negative results are noninformative. However, these limitations emphasize the robustness of positive observations as reported.

CONCLUSIONS

Altogether, stepwise proteomic analyses of cMVs detected prestroke pathway changes (ischemia, BBB-integrity, angiogenesis pathways) associated with stroke susceptibility and pathway changes associated with age- and sex-specific changes (glycolytic pathways, cell-microenvironment interactions, and transendothelial migration pathways). These observations suggest that a paradigm shift toward the prestroke stage could be central to overcoming the "translational roadblock to effective stroke therapies" (2). Observed prestroke pathway changes provide *a priori* putative targets for new diagnostic and therapeutic approaches, and can also give critical pathophysiological context to help address the current conundrum of "Janus-faced stroke treatment targets which have limited efficacy combined with serious side effects" (2).

ACKNOWLEDGMENTS

Grant funding from the National Institutes of Health, RO1 AG32649-02 to VLM Herrera; Whitaker Cardiovascular Institute T32 HL07224 to A Bergerat.

DISCLOSURES

The authors declare that they have no competing interests as defined by *Molecular Medicine*, or other interests that might be perceived to influence the results and discussion reported in this paper.

REFERENCES

1. Dahlof B. (2007) Prevention of stroke in patients with hypertension. *Am. J. Cardiol*. 100(Suppl): 17J–24J.
2. Endres M, *et al*. (2008) Improving outcome after stroke: overcoming the translational roadblock. *Cerebrovasc. Dis*. 25:268–78.
3. Hawkins BT, Davis TP. (2005) The blood brain barrier neurovascular unit in health and disease. *Pharmacol. Rev*. 37:173–85.
4. del Zoppo GJ, Milner R. (2006) Integrin-matrix interactions in the cerebral microvasculature. *Arterioscler. Thromb. Vasc. Biol*. 26:1966–75.
5. Lee SH, *et al*. (2004) Cerebral microbleeds are regionally associated with intracerebral hemorrhage. *Neurology*. 62:72–6.
6. Alemany M, Stenborg A, Terent A, Sonninen P, Raininko R. (2006) Coexistence of microhemorrhages and acute spontaneous brain hemorrhage: correlation with signs of microangiopathy and clinical data. *Radiology*. 238:240–7.
7. Boulanger JM, *et al*. (2006) Cerebral microhemorrhages predict new disabling or fatal strokes in patients with acute ischemic stroke or transient ischemic attack. *Stroke*. 37:911–4.
8. Decano JL, *et al*. (2009) Early-life sodium exposure unmasks susceptibility to stroke in hyperlipidemic, hypertensive heterozygous Tg25 rats transgenic for human cholesteryl ester transfer protein. *Circulation*. 119:1501–9.
9. Hamann GF, Okada Y, del Zoppo GJ. (1996) Hemorrhagic transformation and microvascular integrity during focal cerebral ischemia/reperfusion. *J. Cereb. Blood Flow Metab*. 16:1373–8.
10. Rhodes JM, Simons M. (2007) The extracellular matrix and blood vessel formation: not just a scaffold. *J. Cell Mol. Med*. 11:176–205.
11. Wang CX, Shuaib A. (2007) Critical role of microvasculature basal lamina in ischemic brain injury. *Prog. Neurology*. 83:140–8.
12. Haqqani AS, *et al*. (2005) Characterization of vascular protein expression patterns in cerebral ischemia/reperfusion using laser capture microdissection and ICAT-nanoLC-MS/MS. *FASEB J*. 19:1809–21.
13. Soreghan BA, *et al*. (2005) Using proteomics and network analysis to elucidate the consequences of synaptic protein oxidation in a PS1+AβPP mouse model of Alzheimer's disease. *J. Alzheimers Dis*. 8:227-41.
14. Calabria AR, Shusta EV. (2006) Blood-brain barrier genomics and proteomics: elucidating phenotype, identifying disease targets and enabling brain drug delivery. *Drug Discov. Today*. 11:792–9.
15. del Zoppo GJ. (2010) The neurovascular unit in the setting of stroke. *J. Intern. Med*. 267:156–71.
16. Herrera VL, *et al*. (2004) Analysis of gender-specific atherosclerosis susceptibility in transgenic[hCETP]25DS rat model. *Atherosclerosis*. 177:9–18.
17. Song L, Pachter JS. (2003) Culture of murine brain microvascular endothelial cells that maintain expression and cytoskeletal association of tight junction-associated proteins. *In Vitro Cell. Dev. Biol. Anim*. 39:313–20.
18. Ahmad QR, Nguyen DH, Wingerd MA, Church GM, Steffen MA. (2005) Molecular weight assessment of proteins in total proteome profiles using 1D-PAGE and LC/MS/MS. *Proteome Sci*. 3:6.
19. Peng J, Elias JE, Thoreen CC, Licklider LJ, Gygi SP. (2003) Evaluation of multidimensional chromatography coupled with tandem mass spectrometry (LC/LC-MS/MS) for large-scale protein analysis: the yeast proteome. *J. Proteome Res*. 2:43–50.
20. Wu CJ, *et al*. (2009) A predictive phosphorylation signature of lung cancer. *PlosOne*. 4:e7994.
21. Kumar N, Wolf-Yadlin A, White FM, Lauffenburger DA. (2007) Modeling HER2 effects on cell behavior from mass spectrometry phosphotyrosine data. *PLoS Comput. Biol*. 3:e4.
22. Subramanian A, *et al*. (2005) Gene set enrichment analysis: a knowledge-based approach for interpreting genome-wide expression profiles. *Proc. Natl. Acad. Sci. U. S. A*. 102:15545–50.
23. Choi H, Fermin D, Nesvizhskii AI. (2008) Significance analysis of spectral count data in label-free shotgun proteomics. *Mol. Cell. Proteomics*. 7:2373–85.
24. Kass RE, Raftery AE. (1995) Bayes Factors. *J. Am. Stat. Assoc*. 90:773–95.
25. Jeffreys H. (1961) *The Theory of Probability*. Oxford University Press, 1961, p 432.
26. Ballabh P, Braun A, Nedergaard M. (2004) The blood brain barrier: an overview: structure, regulation, and clinical implications. *Neurobiol. Dis*. 16:1–13.
27. Agarwal N, Lippmann ES, Shusta EV. (2010) Identification and expression profiling of blood brain barrier membrane proteins. *J. Neurochem*. 112:625–35.
28. Liu H, Sadygov RG, Yates JR. (2004) A model for random sampling and estimation of relative protein abundance in shotgun proteomics. *Anal. Chem*. 76:4193–201.
29. Amiry-Moghaddam M, *et al*. (2004) Alpha syntrophin deletion removes the perivascular but not endothelial pool of aquaporin-4 at the blood brain barrier. *FASEB J*. 18:542–4.
30. Bolanos JP, Almeida A, Moncada S. (2010) Glycolysis: a bioenergetic or a survival pathway? *Trends Biochem. Sci*. 35:145–9.
31. Zlokovic BV. (2008) The blood-brain barrier in health and chronic neurodegenerative disorders. *Neuron*. 57:178–201.
32. Verkman AS. (2009) Knock-out models reveal new aquaporin 4 functions. In E. Beitz (ed), Aquaporins, *Handb. Exp Pharmacol*. 190:359–81.
33. Nagelhus EA, Mathiisen TM, Ottersen OP. (2004) Aquaporin-4 in the central nervous system: cellular and subcellular distribution and coexpression with Kir4.1. *Neuroscience*. 129:905–13.
34. Nicchia GP, *et al*. (2004) The role of aquaporin-4 in the blood-brain barrier development and integrity: studies in animal and cell culture models. *Neuroscience*. 129:935–45.
35. Tomassoni D, Bramanti V, Amenta F. (2010) Expression of aquaporins 1 and 4 in the brain of spontaneously hypertensive rats. *Brain Res*. 1325:155–63.
36. Aoki K, *et al*. (2003) Enhanced expression of aquaporin 4 in human brain with infarction. *Acta. Neuropathol*. 106:121–4.
37. Bufa FM, Harris AL, West CM, Miller CJ. (2010) Large meta-analysis of multiple cancers reveals a common, compact and highly prognostic hypoxia metagene. *Br. J. Cancer*. 102:428–35.
38. Gavard J, Gutkind JS. (2008) Protein kinase C-related kinase and ROCK are required for thrombin-induced endothelial cell permeability downstream from Galpha12/13 and Galpha11/q. . *Biol. Chem*. 283:29888–96.
39. Jin X, *et al*. (2003) Shear stress-induced collagen XII expression is associated with atherogenesis. *Biochem. Biophys. Res. Commun*. 308:152–8.
40. Nogradi A, *et al*. (2003) Up-regulation of cerebral carbonic anhydrase by anoxic stress in piglets. *J. Neurochem*. 85:843–50.
41. Shah GN, *et al*. (2005) Carbonic anhydrase IV and XIV knockout mice: roles of the respective carbonic anhydrases in buffering the extracellular space in brain. *Proc. Natl. Acad. Sci. U. S. A*. 102:16771–6.
42. Jung Kang Y, *et al*. (2004) NHERF2 increases platelet-derived growth factor-induced proliferation through PI-3-kinase/Akt-, and Src family kinase-dependent pathway. *Cell. Signal*. 16:791–800.
43. Thiesen CS, Wahl JK 3rd, Johnson KR, Wheelock MJ. (2007) NHERF links the N-cadherin/catenin complex to the platelet-derived growth factor receptor to modulate the actin cytoskeleton and regulate cell motility. *Mol. Biol. Cell*. 18:1220–32.
44. Terwaki S, Maesaki R, Hakoshima T. (2006) Structural basis for NHERF recognition by ERM proteins. *Structure*. 14:777–89.
45. Rangel R, *et al*. (2007) Impaired angiogenesis in aminopeptidase N-null mice. *Proc. Natl. Acad. Sci. U. S. A*. 104:4588–93.
46. Zeng M, Kikuchi H, Pino MS, Chung DC. (2010) Hypoxia activates the K-ras proto-oncogene to stimulate angiogenesis and inhibit apoptosis in colon cancer cells. *PLoSOne* 5(6):e10966.
47. Del Valle-Perez B, *et al*. (2010) Filamin B plays a key role in VEGF-induced endothelial cell motility through its interaction with Rac-1 and Vav-2. *J. Biol. Chem*. 285:10748–60.
48. Kanters E, *et al*. (2008) Filamin B mediates ICAM-1-driven leukocyte transendothelial migration. *J. Biol. Chem*. 283:31830–9.
49. Moos T, Morgan EH. (2004) The metabolism of neuronal iron and its pathogenic role in neurological disease: review. *Ann. N.Y. Acad. Sci*. 1012:14–26.
50. van Campenhout A, van Campenhout CM, Lagrou AR, Manuel-Y-Keenov B. (2007) Transferrin modifications and lipid peroxidation: implications in diabetes mellitus. *Free Radic. Res*. 37:1069–77.
51. Ponce ML, Kleinman HK. (2003) Identification of redundant angiogenic sites in laminin alpha1 and gamma1 chains. *Exp. Cell Res*. 285:189–95.